Development/Plasticity/Repair

P/Q-Type Ca^{2+} Channel α1A Regulates Synaptic Competition on Developing Cerebellar Purkinje Cells

Taisuke Miyazaki,[1]* Kouichi Hashimoto,[2]* Hee-Sup Shin,[3] Masanobu Kano,[2] and Masahiko Watanabe[1]

[1]Department of Anatomy, Hokkaido University School of Medicine, Sapporo 060-8638, Japan, [2]Department of Cellular Neurophysiology, Graduate School of Medical Science, Kanazawa University, Takara-machi, Kanazawa 920-8640, Japan, and [3]National Creative Research Initiative Center for Calcium and Learning, Korea Institute of Science and Technology, Seongbuk-ku, Seoul 136-791, Korea

Synapse formation depends critically on the competition among inputs of multiple sources to individual neurons. Cerebellar Purkinje cells have highly organized synaptic wiring from two distinct sources of excitatory afferents. Single climbing fibers innervate proximal dendrites of Purkinje cells, whereas numerous parallel fibers converge on their distal dendrites. Here, we demonstrate that the P/Q-type Ca^{2+} channel α1A, a major Ca^{2+} channel subtype in Purkinje cells, is crucial for this organized synapse formation. In the α1A knock-out mouse, many ectopic spines were protruded from proximal dendrites and somata of Purkinje cells. Innervation territory of parallel fibers was expanded proximally to innervate the ectopic spines, whereas that of climbing fibers was regressed to the basal portion of proximal dendrites and somata. Furthermore, multiple climbing fibers consisting of a strong climbing fiber and one or a few weaker climbing fibers, persisted in the majority of Purkinje cells and were cowired to the same somata, proximal dendrites, or both. Therefore, the lack of α1A results in the persistence of parallel fibers and surplus climbing fibers, which should normally be expelled from the compartment innervated by the main climbing fiber. These results suggest that a P/Q-type Ca^{2+} channel α1A fuels heterosynaptic competition between climbing fibers and parallel fibers and also fuels homosynaptic competition among multiple climbing fibers. This molecular function facilitates the distal extension of climbing fiber innervation along the dendritic tree of the Purkinje cell and also establishes climbing fiber monoinnervation of individual Purkinje cells.

Key words: **cerebellum; Purkinje cell; climbing fiber; parallel fiber; P/Q-type calcium channel; α1A subunit; development; synapse formation**

Introduction

The cerebellar cortex receives two excitatory afferents, climbing fibers (CFs) and mossy fibers (Palay and Chan-Palay, 1974). An enormous amount of information is transferred at the mossy fiber–granule cell synapses and then to Purkinje cells (PCs) via parallel fibers (PFs), the granule cell axons. Each PC forms 10^5~10^6 PF synapses on its distal dendrites called spiny branchlets, accounting for >95% of the total PC synapses (Sotelo, 1978). In contrast, each PC is innervated by a single CF, which forms hundreds of synapses onto proximal shaft dendrites. Hence, CF activity can cause strong depolarization of the innervating PCs and trigger Ca^{2+} entry into them through voltage-dependent Ca^{2+} channels (VDCCs) (Kano et al., 1992; Konnerth et al., 1992; Regehr and Mintz, 1994). When coactivated with CFs, PF synapses undergo long-term depression, a form of synaptic plasticity thought to underlie motor learning in the cerebellum (Ito, 2001).

The monoinnervation by CFs is preceded by the stage of multiple innervation. During the first week of the rodent's life, multiple CFs innervate the soma of each PC (Crepel et al., 1981; Mariani and Changeux, 1981a,b) and form the "pericellular nests" (Altman, 1972). During the second week, supernumerary CFs decrease until a one-to-one relationship is achieved. Simultaneously, the pericellular nests are displaced progressively toward "peridendritic" innervation (Chedotal and Sotelo, 1992). Analyses of classical agranular animal models elucidate that PF–PC synaptogenesis is a prerequisite for developmental elimination of surplus CFs (Woodward et al., 1974; Crepel et al., 1980; Mariani, 1982; Bravin et al., 1995; Sugihara et al., 2000). Studies using gene knock-out mice have extended our knowledge that glutamate receptors play important roles in the excitatory synaptic wiring to PCs (Kano et al., 1995, 1997, 1998; Kashiwabuchi et al., 1995; Kurihara et al., 1997; Offermanns et al., 1997; Ichise et al., 2000; Hashimoto et al., 2001; Ichikawa et al., 2002). In particular, the glutamate receptor GluRδ2, although its native ligands and channel properties remain elusive, is crucial for PF–PC synaptogenesis (Guastavino et al., 1990; Kashiwabuchi et al., 1995; Kurihara et al., 1997; Lalouette et al., 2001) and for restricting CF innervation to proximal dendrites (Hashimoto et al., 2001;

Received Sept. 13, 2003; revised Dec. 9, 2003; accepted Dec. 10, 2003.

This work was supported by Grants for Scientific Research on Priority Areas (to M.W., K.H., and M.K.), Special Coordination Funds for Promoting Science and Technology (M.K., K.H.), and a Grant-in-Aid for Scientific Research (M.W., K.H., M.K.) provided by the Ministry of Education, Culture, Sports, Science, and Technology, and the Japanese Government. This work was also supported in part by Takeda Science Foundation (M.W.) and Ichiro Kanehara Foundation (M.W.). We thank Dr. Ryoichi Ichikawa (Sapporo Medical University) for his technical support to anterograde neuronal tracing.

*T.M. and K.H. contributed equally to this work.

Correspondence should be addressed to Masahiko Watanabe, Department of Anatomy, Hokkaido University School of Medicine, Sapporo 060-8638, Japan. E-mail: watamasa@med.hokudai.ac.jp.

DOI:10.1523/JNEUROSCI.4208-03.2004

 0270-6474/04/241734-10$15.00/0

Ichikawa et al., 2002). Thus, the developmental wiring of PFs and that of CFs are competitive with each other, and GluRδ2 supports PF synaptogenesis. Intriguingly, reciprocal changes (i.e., expanded PF innervation and regressed CF innervation) are induced in the adult cerebellum when afferent activities are silenced by tetrodotoxin (Bravin et al., 1999). These results suggest that counter mechanisms that support CFs over PFs in an acitivity-dependent manner should exist to structure properly organized innervation.

To test this hypothesis, we examined the cerebellum lacking the α1A subunit of P/Q-type Ca^{2+} channels. We found that in the α1A knock-out mouse, CF innervation was regressed proximally, whereas PF innervation was expanded reciprocally. Furthermore, multiple CFs persisted in the majority of mutant PCs by innervating the same somatodendritic compartments. Therefore, VDCC α1A subunit consolidates innervation territory by a single main CF and expels surplus CFs and PFs from its territory.

Materials and Methods

Animals and sections. The null knock-out mouse defective in VDCC α1A subunit was produced by homologous recombination as described previously (Jun et al., 1999). Heterozygous pairs were mated to obtain the homozygous mutant ($\alpha1A^{+/+}$) and control ($\alpha1A^{-/-}$) offspring. The genotype was determined by PCR using a mixture of primers CCa1AF1 (5′-ataataagtcacctctcgttctaaag-3′), CCa1AR1 (5′-ccagcttgagtggccgcagcacacg-3′), and PGK-neo (5′-ctgactaggggaggagtagaag-3′), which yields cDNA fragments of 280 and 360 base pairs for the wild-type or knock-out allele, respectively.

In each morphological analysis, we used three mutant and three control mice at postnatal day (P) 21 unless otherwise noted. Under deep pentobarbital anesthesia, mice for light microscopic analyses (i.e., histology, immunohistochemistry, and anterograde tracer labeling) were perfused transcardially with 4% paraformaldehyde in 0.1 M sodium phosphate buffer, pH 7.2. After excision from the skull, brains were further immersed overnight in the same fixative and processed for preparation of parasagittal microslicer sections (50 μm in thickness; VT1000S; Leica, Wien, Austria) or for parasagittal paraffin sections (4 μm; SM2000R, Leica). For conventional electron microscopy, mice were perfused with 2% paraformaldehyde–2% glutaraldehyde in 0.1 M sodium cacodylate buffer, pH 7.2. Microslicer sections (400 μm) were postfixed with 1% osmium tetroxide in 0.1 M cacodylate buffer for 1 hr, dehydrated in graded alcohols, and embedded in Epon 812 for the preparation of ultrathin sections (70 nm in thickness) using an Ultracut ultramicrotome (Leica).

Antibody. We used rabbit calbindin antiserum (1:10,000), guinea pig vesicular glutamate transporter 1 (VGluT1) antibody (1 μg/ml), and guinea pig VGluT2 antibody (1 μg/ml), the specificities of which have been reported previously (Nakagawa et al., 1998; Miyazaki et al., 2003). For immunofluorescence, FITC-, indocarbocyanine-, and aminomethylcoumarin acetate-labeled species-specific secondary antibodies were used at a dilution of 1:200 (Jackson Immunoresearch, West Grove, PA). For immunoperoxidase, immunoreaction was visualized with 3,3′-diaminobenzidine (DAB) using a Histofine SAB-PO(R) kit (Nichirei, Tokyo, Japan).

Histology. A midsagittal microslicer section was selected from each mouse such that the section had the smallest medullar zone at the base of the cerebellar lobules. After staining with hematoxylin, images of the cerebellar histology were taken with a light microscope (AX-70; Olympus Optical, Tokyo, Japan) equipped with a digital camera DP11 (Olympus Optical).

Immunofluorescence. Microslicer sections were immunoreacted overnight with calbindin antiserum, followed by incubation with fluorescent secondary antibody for 2 hr. Images were taken with a confocal laser-scanning microscope (Fluoview, Olympus Optical). To quantitatively evaluate somatic association or dendritic translocation of CFs, double immunofluorescence for calbindin and VGluT2 was applied to paraffin sections at P10, P15, P18, and P21, and images were taken with a fluorescence microscope (AX-70, Olympus Optical) equipped with a CCD camera (Sensys; Nippon Roper, Chiba, Japan) and analyzed with Metamorph software (Nippon Roper). Somatic association by CFs was judged by the presence of at least three VGluT2-positive puncta on the somatic surface of PCs. Dendritic translocation of CFs was evaluated by measuring the distance from the base of the molecular layer to the tips of VGluT2-positive puncta relative to the total vertical length of the molecular layer.

Electron microscopy. For qualitative and quantitative analyses by conventional electron microscopy, ultrathin sections cut in the parasagittal or transverse plane were prepared from the straight portion of the lobules 4/5 and stained with 2% uranyl acetate for 5 min and mixed lead solution for 2 min. In each mouse, 10 electron micrographs were taken randomly from the neuropil of the molecular layer. In addition, 10 electron micrographs containing thick PC dendrites (>2 μm in caliber) were taken from each mouse to measure the spine formation at proximal shaft dendrites. All electron micrographs were taken at an original magnification of 4000× and printed at the final magnification of 16,000×. For immunoperoxidase electron microscopy, microslicer sections that had been immunoreacted with VGluT1 or VGluT2 antibody and visualized with DAB were postfixed with 1% osmium tetroxide in 0.1 M cacodylate buffer for 15 min, dehydrated in graded alcohols, and embedded in Epon 812.

Anterograde labeling. Under anesthesia with chloral hydrate (350 mg/kg of body weight, i.p.), a glass pipette (G-1.2; Narishige, Tokyo, Japan) filled with 2–3 μl of 10% solution of biotinylated dextran amine [BDA; 10,000 molecular weight (MW); Molecular Probes, Eugene, OR] or dextran Texas red (DTR; 3000 MW; Molecular Probes) in PBS, pH 7.4, was inserted stereotaxically to the inferior olive by the dorsal approach. The tracer was injected by air pressure at 20 psi with 5 sec intervals for 1 min (Pneumatic Picopump; World Precision Instruments, Tokyo, Japan). After 2 d of survival, mice were anesthetized and fixed by transcardial perfusion.

For bright-field light microscopy, BDA-labeled CFs were visualized by overnight incubation with avidin-biotin-peroxidase complex (Elite ABC kit; Vector Laboratories, Burlingame, CA) and colored in black using DAB and cobalt. Some sections were further processed for immunoperoxidase for calbindin to label PCs with brown DAB products. For fluorescence microscopy by combined anterograde and immunofluorescence labelings, DTR-labeled microsclicer sections were incubated with calbindin antiserum or with a mixture of calbindin antiserum and VGluT2 antibody followed by incubation with fluorescent secondary antibodies for 2 hr. Images of double labeling were taken with a confocal laser-scanning microscope, and those of triple labeling were taken with a fluorescence microscope and deconvoluted using MetaMorph (Nippon Roper) and AutoDeblur software (AutoQuant, Watervliet, NY).

For electron microscopy by combined anterograde and immunoelectron labelings, BDA-labeled microslicer sections were incubated overnight with a mixture of VGluT2 antibody and avidin-biotin-peroxidase complex, which were diluted with Tris-buffered saline containing 1% BSA and 0.004% saponin. Sections were then incubated with 1.4 nm gold particle-conjugated anti-guinea pig antibody (1:200; Nanogold; Nanoprobes, Stony Brook, NY) for 3 hr. Immunogold for VGluT2 was first silver-enhanced using an HQ-silver enhance kit (Nanoprobes), and then BDA was visualized with DAB. Sections were postfixed with 1% osmium tetroxide for 15 min, dehydrated in graded alcohols, and embedded in Epon 812. Serial ultrathin sections were prepared in the transverse plane (i.e., parallel to the pial surface to reconstruct innervation patterns from the base of Purkinje cell dendrites upwards).

Electrophysiology. Parasagittal cerebellar slices (250 μm thickness) were prepared from wild-type ($\alpha1A^{+/+}$), heterozygous ($\alpha1A^{+/-}$), and homozygous mutant ($\alpha1A^{-/-}$) mice P18–P29 as described previously (Kano et al., 1995, 1997). Because we have not found any electrophysiological difference so far between $\alpha1A^{+/+}$ and $\alpha1A^{+/-}$ mice, we used both genotypes as controls in electrophysiological analyses. Whole-cell recordings were made from visually identified PCs using an upright microscope (BX51WI; Olympus Optical) at 31°C. Resistances of patch pipettes were 3–6 MΩ when filled with an intracellular solution composed of (in mM): 60 CsCl, 10 Cs D-gluconate, 20 TEA-Cl, 20 BAPTA, 4 $MgCl_2$, 4 ATP, 0.4 GTP, and 30 HEPES, pH 7.3, adjusted with CsOH. The pipette access resistance was compensated by 70–80%. The composition of the standard bathing solution was (in mM): 125 NaCl, 2.5 KCl, 2 $CaCl_2$, 1 $MgSO_4$, 1.25 NaH_2PO_4, 26 $NaHCO_3$, and 20 glucose, bubbled with 95%

O_2 and 5% CO_2. Bicuculline (10 μM) was always added to block inhibitory synaptic transmission. Ionic currents were recorded with an Axopatch 1D (Axon Instruments, Foster City, CA) patch-clamp amplifier. The signals were filtered at 2 kHz and digitized at 20 kHz. On-line data acquisition and off-line data analysis were performed using PULSE software (Heka Elektronik, Lambrecht/Pfalz, Germany). Stimulation pipettes (5–10 μm tip diameter) were filled with standard saline and used to apply square pulses for focal stimulation (duration, 0.1 msec; amplitude, 0–90 V). CFs were stimulated in the granule cell layer 50–100 μm away from the Purkinje cell soma.

Results

Hyperspiny transformation and altered synaptic morphology

As reported previously (Jun et al., 1999), the mutant cerebellum defective in VDCC α1A subunit was slightly reduced in size but grossly normal in the cerebellar anatomy, including the foliation, laminated organization, and monolayer alignment of PCs (Fig. 1*A*,*C*). Immunofluorescence for calbindin demonstrated that the soma and proximal shaft dendrites of mutant PCs often had a rough surface, in contrast to the smooth surface of control PCs (Fig. 1*B*,*D*). Electron microscopy demonstrated that the rough surface resulted from ectopic formation of numerous spines or spine-like protrusions from the soma and proximal dendrites (Fig. 1*E*,*F*). This hyperspiny transformation was quantitatively evaluated; the number of spines per micrometer of proximal dendrites (>2 μm in caliber) showed a significant fourfold increase in the mutant mouse, being 0.065 ± 0.084 in the control mouse and 0.240 ± 0.107 in the mutant mouse (Fig. 1*I*) (mean ± SD; $n = 3$; *t* test; $p < 0.0001$).

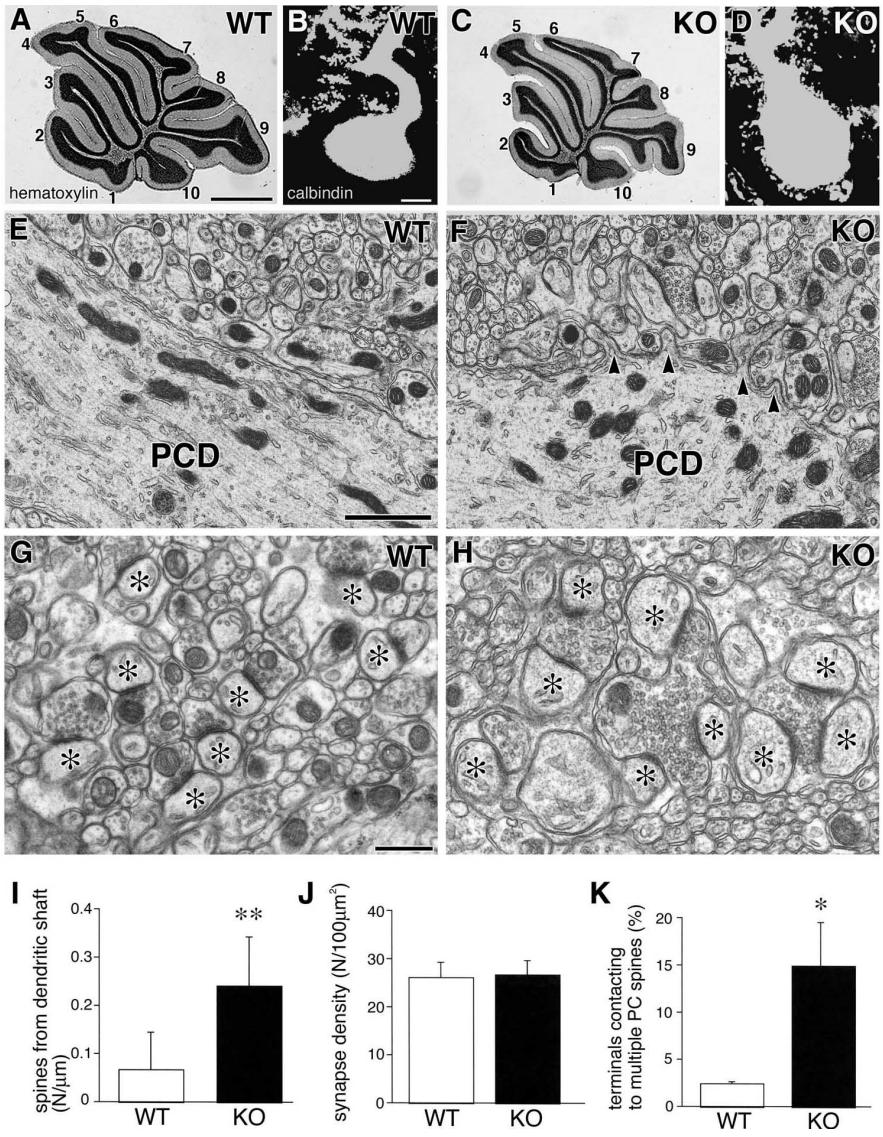

Figure 1. *A–H*, Cerebellar histology and Purkinje cell cytology in the VDCC α1A control (*A*, *B*, *E*, *G*) and mutant (*C*, *D*, *F*, *H*) mice. *A*, *C*, Hematoxylin staining for midsagittal cerebellar sections. The lobule number is indicated by the numbers 1–10. *B*, *D*, Calbindin immunofluorescece. *E–H*, Electron micrographs of proximal shaft dendrites of PCs (*E*, *F*) and PC synapses in the neuropil (*G*, *H*). Arrowheads indicate the neck of ectopic spines protruding from a shaft dendrite of a mutant. Asterisks indicate the head of PC spines forming asymmetric contact with axon terminals. *I--K*, Histograms showing the spine number per 1 μm of proximal shaft dendrites (*I*), the number of junctions at axo-spinous synapses per 100 μm^2 of the neuropil (*J*), and the percentage of axon terminals contacting multiple spines (*K*). *$p < 0.005$; **$p < 0.0001$. WT, Wild-type; KO, knock-out; PCD, Purkinje cell dendrite. Scale bars: *A*, 1 mm; *B*, 20 μm; *E*, 1 μm; *G*, 500 mm.

In both strains of mice, spines forming asymmetrical synapses (i.e., excitatory synapses on PCs) were distributed in large numbers in the neuropil of the molecular layer (Fig. 1*G*,*H*). No significant difference was found in the number of axo-spinous synapses per 100 μm^2 of the neuropil, being 26.5 ± 3.7 in the control mouse and 27.0 ± 3.7 in the mutant mouse (Fig. 1*J*) ($n = 3$; $p = 0.856$). However, their morphology was altered conspicuously. First, most axo-spinous synapses in the control mouse had a contact ratio of 1:1 between terminals and PC spines, and only a minor population had a contact ratio of 1:2 (i.e., synapses with a single terminal connecting to two spines) (Fig. 1*G*). In contrast, axo-spinous synapses in the mutant mouse often had multiple contact ratios, ranging from 1:2 to 1:6 (Fig. 1*H*). On electron micrographs, the percentage of axo-spinous synapses with multiple contact ratios was 2.4 ± 1.0% in the control mouse and 14.9 ± 4.9% in the mutant mouse, indicating a significant increase in the mutant mouse (Fig. 1*K*) ($n = 3$; $p < 0.005$). Second, in the control mouse, terminals forming axo-spinous synapses were small in size (0.5–1 μm), oval in shape, and contained relatively few synaptic vesicles accumulating near the synaptic junction. In contrast, those in the mutant mouse were often enlarged (>1 μm), had densely accumulated synaptic vesicles, and exhibited an irregular contour attributable to the attachments by multiple spines (Fig. 1*H*). These results indicate that the lack of the VDCC α1A subunit induces ectopic spine formation at the proximal somatodendritic domain of PCs and alters the morphology of excitatory PC synapses.

Proximal expansion of PF innervation territory

Conventional morphological criteria are that small terminals connecting to single spines originate from parallel fibers, whereas large terminals with multiple contacts to spines and containing numerous vesicles are from climbing fibers (Palay and Chan-

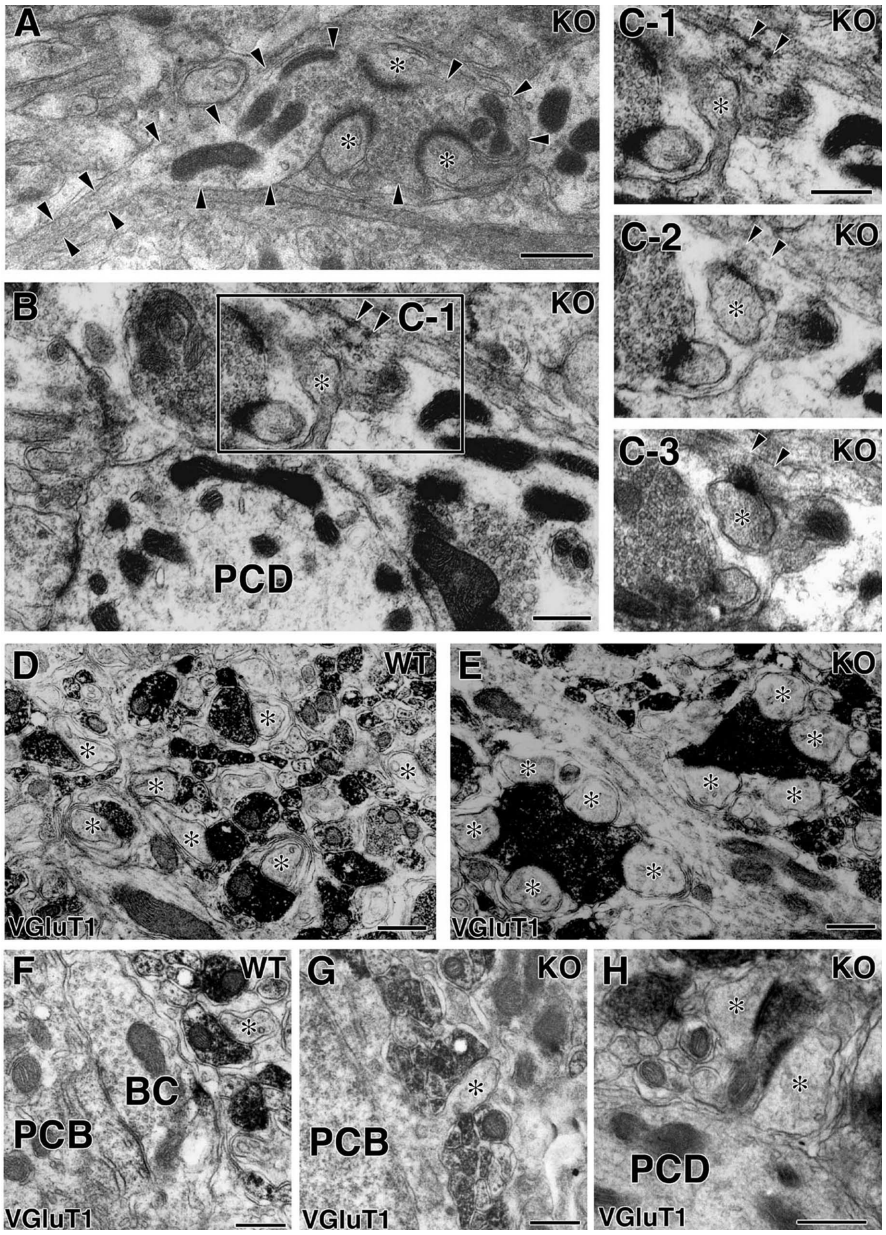

Figure 2. Altered terminal morphology of PFs in the neuropil and their innervation of ectopic spines protruding from PC somata and proximal dendrites. *A–C*, Conventional electron microscopy for the mutant cerebellum sectioned in the transverse plane. In *A*, arrowheads indicate the contour of a PF, which is cut longitudinally and forms a large terminal swelling contacting to several spines (*). *C1–C3* are serial micrographs corresponding to the boxed region of *B*, in which a spine from the proximal PC dendrite (PCD) is innervated by a longitudinal PF (arrowheads). *D–H*, Immunoelectron microscopy for VGluT1 in the control (*D*, *F*) and mutant (*E*, *G*, *H*) mice. Asterisks indicate PC spines forming asymmetric contact with VGluT1-positive PF terminals. WT, Wild-type; KO, knock-out; BC, axon terminal of the basket cell; PCB, Purkinje cell body. Scale bars, 500 nm.

Palay, 1974). Because these criteria seemed inapplicable to the VDCC α1A mutant mouse, PF innervation was examined by electron microscopy with serial transverse sections cut parallel to the pial surface (Fig. 2*A–C*). In addition, PFs were identified by their immunoreactivity to vesicular glutamate transporter VGluT1 (Fig. 2*D–H*), a molecule localized at PF terminals but not at CF terminals (Fremeau et al., 2001; Miyazaki et al., 2003).

In the control mouse, individual PF terminals identified by electron microscopy as small oval bulgings on transverse axons formed asymmetrical contacts primarily with single spines on spiny branchlets (data not shown). These terminals were immunopositive for VGluT1 (Fig. 2*D*), further confirming that they were PFs. In the mutant mouse, terminals on such transverse axons also had VGluT1 immunoreactivity but frequently contacted with several spines (Fig. 2*A*, *E*, asterisks). This observation indicates that a substantial fraction of axo-spinous synapses with multiple contact ratios are indeed PF synapses. Moreover, we found that PF terminals innervated ectopic spines on PC somata and proximal dendrites in the mutant mouse (Fig. 2*B*,*C*,*G*,*H*). In contrast, spines on proximal dendrites of the control mouse were innervated by CFs, which ascended along shaft dendrites and were immunopositive to VGluT2, another transporter subtype localized to CF terminals (data not shown). In addition, somata of control PCs had no spines and were fully covered by either basket cell terminals or Bergmann glial processes (Fig. 2*F*). These results indicate that the lack of VDCC α1A subunit results in a significant expansion of the PF innervation territory, down to proximal dendrites and even to the soma of PCs.

Diminished extent of CF innervation territory

CF innervation was examined by injecting the following anterograde tracers to the inferior olivary nucleus in the medulla: BDA for light and electron microscopies and DTR for fluorescence and confocal laser-scanning microscopies. In the control mouse, CFs were extended to approximately four-fifths of the molecular layer without forming terminals at the level of PC somata (Fig. 3*A–C*). In contrast, CFs of the mutant mouse were stunted and poorly arborized in the molecular layer, and formed ectopic terminals around the PC somata (Fig. 3*D–F*). Immunoperoxidase electron microscopy revealed that BDA-labeled CFs formed large terminal swellings at the somatic level and contacted to somatic spines in the mutant mouse (Fig. 3*H*), whereas CFs in the control mouse only passed by the perisomatic space (Fig. 3*G*). This phenotypic difference was also depicted by immunofluorescence microscopy for calbindin and VGluT2 (Fig. 3*I*,*J*). A majority of the PC somata (71.6 ± 7.3%) in the mutant mouse was associated with VGluT2-positive terminals, whereas such perisomatic terminals were far less distributed around PC somata (6.7 ± 1.2%) in the control mouse, showing a significant difference ($n = 3$; $p < 0.0001$). Because somatic innervation by CFs is normally seen in neonates, we examined whether the phenotype of this mutant resulted from impaired developmental elimination of somatic CF synapses. In both mice, all of the PC somata were associated with VGluT2-positive puncta at P10. Thereafter, the percentage of somata associated with VGluT2-positive

puncta was reduced progressively to 52.3 ± 6.8% at P15 and 13.4 ± 7.6% at P18 in the control mouse, whereas it remained as high as 93.1 ± 4.7% at P15 and 83.7 ± 2.2% at P18 in the mutant mouse, showing significant differences ($n = 3$ for each; $p < 0.001$ at P15; $p < 0.0001$ at P18).

We then compared patterns of dendritic CF innervation by double fluorescent labeling for DTR (Fig. 3*K*,*L*, red) and calbindin (green). In the control mouse, DTR-labeled CFs climbed and branched along with proximal dendrites and reached their transition to spiny branchlets (Fig. 3*K*). In the mutant mouse, DTR-labeled CFs abruptly stopped their association in the midst of proximal dendrites and left the remaining portions free of CF innervation (Fig. 3*L*, arrowheads). This incomplete invasion of CFs to PC dendrites was also reflected in the lowered vertical height of VGluT2-labeled CF terminals; the mean relative height to the most distal terminals was 78.6 ± 4.5% in the control molecular layer and 60.8 ± 9.0% in the mutant layer, showing a significant difference ($n = 3$; $p < 0.0001$). These results indicate that loss of the VDCC α1A subunit results in the persistence of somatic innervation by CFs and insufficient distal extension of the CF territory along PC dendrites.

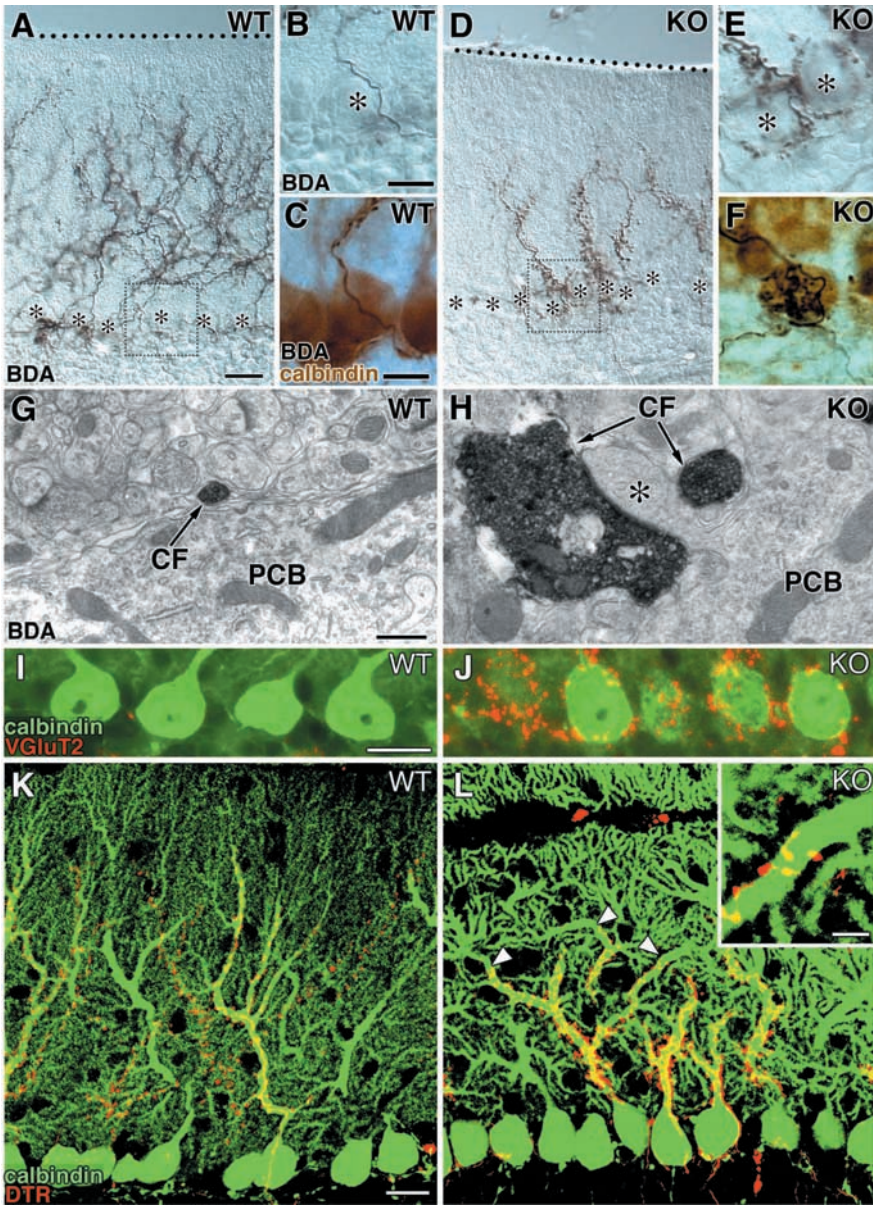

Figure 3. Aberrant somatic innervation and stunted dendritic innervation by CFs in the α1A mutant PCs. *A–F*, Anterograde labeling of CFs by BDA. Dotted line in *A* and *D* indicates the pial surface. Asterisks in *A*, *B*, *D*, and *E* indicate the soma of PCs. High-power micrographs of *B* and *E* correspond to the boxed regions in *A* and *D*, respectively. In *C* and *F*, PC somata are visualized by calbindin immunoperoxidase (brown) in addition to black BDA labeling for CFs. *G*, *H*, Electron microscopy for BDA-labeled CFs. CFs innervate somatic spines (*) in the mutant (*H*) but not in the control mouse (*G*). *I*, *J*, Fluorescence microscopy for calbindin (green) and VGluT2 (red). Dense association of VGluT2-positve terminals is seen around somata of mutant PCs. *K*, *L*, Confocal microscopy for fluorescent anterograde tracer DTR (red) and calbindin (green). Arrowheads in *L* indicate the abrupt stop of CF innervation, leaving the remainder of the shaft dendrites free of CF innervation. WT, Wild-type; KO, knock-out; PCB, Purkinje cell body. Scale bars: *A*, *I*, *K*, 20 μm; *B*, *C*, inset in *L*, 10 μm; *G*, 500 nm.

High degree of persistent multiple CF innervation

We next examined whether the elimination of supernumerary CF synapses occurs normally during cerebellar development. We estimated the number of CFs innervating each PC through electrophysiological examination (Kano et al., 1995, 1997; Kakizawa et al., 2003). In cerebellar slices from control and mutant mice at P18–P29, we conducted whole-cell recordings from visually identified PCs and stimulated the CFs in the granule cell layer. When a CF was stimulated, an EPSC was elicited in an all-or-none manner in the majority of control PCs (Fig. 4*A*, top), indicating that these PCs are innervated by single CFs (termed CF-mono). In some PCs, more than one discrete CF-mediated EPSC (CF-EPSC) could be elicited when the CF-stimulating electrode was moved systematically by 20 μm step, and the stimulus intensity was increased gradually at each stimulation site. The number of CFs innervating the PC was estimated by counting the number of discrete CF-EPSC steps. The summary graph in Figure 4*B* indicates that 75.0% (39 of 52) of the PCs were innervated by single CFs in the control mouse. In contrast, two or more discrete CF-EPSCs were elicited in the majority (83.7%; 72 of 86) of the PCs in the mutant mouse (Fig. 4*A*, bottom). These results clearly indicate that developmental elimination of redundant CF wiring is severely impaired in the VDCC α1A mutant mouse.

Mutant PCs innervated by multiple CFs typically had one strong CF that generated large EPSC (termed CF-multi-S) plus one or a few weaker CFs that elicited smaller EPSCs (termed CF-multi-W) (Fig. 4*A*, bottom). This is similar to the multiply innervated PCs of wild-type mice during the second and third postnatal weeks (Hashimoto and Kano, 2003). This result suggests that multiple CFs on individual PCs are differentiated into one CF with the strongest innervation and other CFs with weaker innervation, despite the lackof α1A.

Redundant CF wiring to the same somatodendritic domain

To examine patterns of multiple CF innervation, we used triple fluorescent labeling for DTR (red), VGluT2 (green), and calbindin (blue) (Fig. 5). We collected PCs that were innervated by

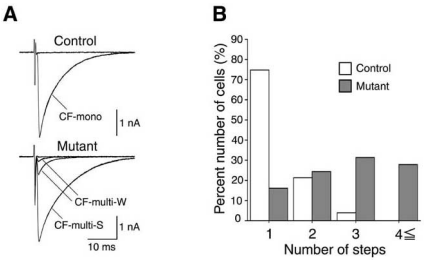

Figure 4. Persistent multiple CF innervation of PCs in mutant mice. *A*, CF-EPSCs recorded in a PC from a control mouse (P29; top panel) and a mutant mouse (P19; bottom panel). CFs were stimulated in the granule cell layer at 0.2 Hz. Two to three traces are superimposed at each threshold stimulus intensity. Holding potential was −20 mV. The control PC was innervated by a single CF (CF-mono), whereas the mutant PC was innervated by a CF that generated a large EPSC (CF-multi-S) and two additional CFs that elicited much smaller EPSCs (CF-multi-W). *B*, Summary histograms showing the number of discrete steps of CF-EPSCs from control mice (open columns; 4 mice, 52 PCs) and from mutant mice (filled columns; 7 mice, 86 PCs).

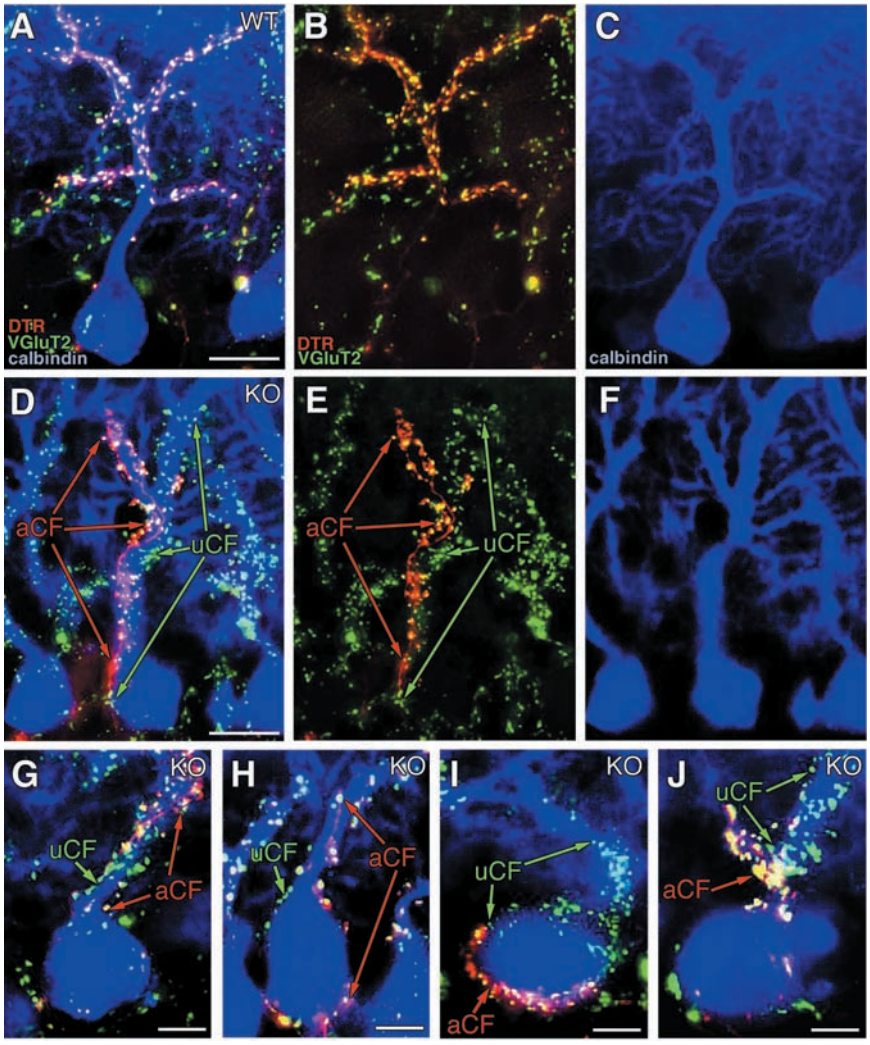

Figure 5. *A–J*, Triple fluorescent labeling demonstrating single CF innervation in the control mouse (*A–C*) and multiple CF innervation in the mutant mouse (*D–J*). Triple labelings for DTR (red), VGluT2 (green), and calbindin (blue) are shown as merged images (*A*, *D*, *G–J*) or separate images (*B*, *C*, *E*, *F*). Throughout the panels, aCF and uCF represent anterogradely labeled or unlabeled CF, respectively. WT, Wild-type; KO, knock-out. Scale bars: *A*, *D*, 20 μm; *G--J*, 10 μm.

DTR-labeled CFs and whose somata and proximal dendrites were continuously traced by calbindin immunofluorescence ($n = 21$ for control, and $n = 24$ for mutant). In the control mouse, CF terminals labeled for DTR were overlapped almost completely with VGluT2 in all PCs examined (21 of 21 PCs) (Fig. 5*A–C*), indicating that multiply innervated PCs could not be detected by our morphological examination. In contrast, the soma and proximal dendrites of most mutant PCs (22 of 24; 92%) were associated with DTR-unlabeled/VGluT2-labeled terminals [anterogradely unlabeled CFs (uCF)], in addition to DTR-labeled/VGluT2-labeled terminals [i.e., anterogradely labeled CFs (aCF)] (Fig. 5*D–J*). In all of these multiply innervated PCs, aCF and uCF were associated more or less with the same somatodendritic compartments, at somata (4 of 22), proximal dendrites (17 of 22), or both (1 of 22). In Figure 5*D–F*, aCF and uCF innervated the same soma and primary dendrite; the former climbed up further, primarily along the left branch of the secondary dendrites, whereas the latter rose along the right branch. The four other examples shown in Figure 5*G–J*, exhibited multiple innervation by aCF and uCF with their uneven extents of somatodendritic association. In these cases, aCF were associated with the PCs to a greater extent than uCF (Fig. 5*G*,*H*) or vice versa (Fig. 5*I*,*J*). Furthermore, termination sites for aCF and uCF tended to segregate locally from each other within the same compartments; they formed terminals on different somatic hemispheres (Fig. 5*H*,*I*), dendritic facets (Fig. 5*D*), or dendritic portions (Fig. 5*D*,*G*,*J*). These results suggest that a majority of α1A mutant PCs receive mixed innervation by multiple CFs at the same somatodendritic compartments, showing some differences in dominance and tendency to segregate in local termination.

The mixed innervation was further substantiated by double labeling electron microscopy for BDA (diffuse immunoperoxidase products) and VGluT2 (deposits of metal particles) (Fig. 6*A–C*). By preparing serial transverse sections, we followed proximal dendrites from their base up to approximately half the height of the molecular layer (Fig. 6*D*). Spines from the basal portions of proximal dendrites were innervated by BDA-labeled/VGluT2-labeled CF (Fig. 6*A–C*, aCF; Fig. 6*D*, red spots), BDA-unlabeled/VGluT2-labeled CF (uCF, green spots), and BDA-unlabeled/VGluT2-unlabeled terminals on transverse axons (i.e., PF terminals) (Fig. 6*D*, yellow spots). In this case, uCF innervated the basal portions of proximal dendrites to a larger extent than the aCF. From the fact that proximal dendrites are innervated by single CFs but not by PFs in the adult wild-type PCs (Larramendi and Victor, 1967; Ichikawa et al., 2002), it is deduced that the mixed innervations over the same dendrites (and even somata) by multiple CFs and ectopic PFs are the conspicuous features in the VDCC α1A knock-out mouse.

Basic properties of CF-EPSC and PF-mediated EPSC

Finally, we examined the basic properties of excitatory synaptic transmission. The 10–90% rise time, decay time constant, and chord conductance of CF-EPSC were similar between the control

and mutant mice (Table 1), although the 10–90% rise time and decay time constant for CF-multi-S were slightly longer in the mutant mouse (Table 1). CF-EPSCs displayed paired-pulse depression at interpulse intervals of 10–3000 msec in both control and mutant mice. There was no difference in the extent of paired-pulse depression between CF-mono of the control mouse and CF-multi-S of the mutant mouse (Fig. 7*A*). The extent of depression for CF-multi-W tended to be larger than that for CF-multi-S in the mutant mouse (Fig. 7*A*). This is analogous to the difference in paired-pulse depression between the strong and weaker CFs of multiply innervated PCs during the second and third postnatal weeks of normal development (Hashimoto and Kano, 2003). Matsushita et al. (2002) made electrophysiological characterization of CF-EPSCs from the two strains of mice with spontaneous mutation of the α1A gene, tottering and rolling Nagoya. They reported that the extent of paired-pulse depression was smaller in the tottering, whereas the amplitude was larger and the decay time constant was longer in the rolling Nagoya when compared with the control mice (Matsushita et al., 2002). Other aspects of CF-EPSC were normal in these two spontaneous mutant mice (Matsushita et al., 2002). In terms of cerebellar ataxia, the order of severity is: tottering less than rolling Nagoya less than the α1A knock-out mouse. Thus, the severity of ataxia does not simply correlate with the changes in the electrophysiological properties of CF-EPSC.

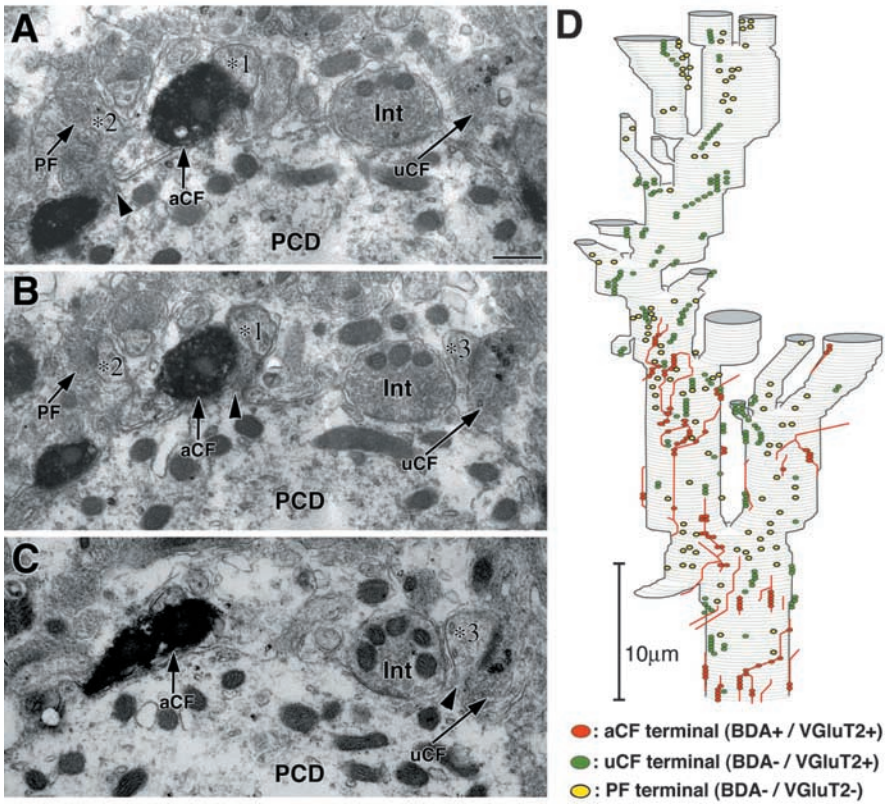

Figure 6. Serial electron micrographs demonstrating mixed innervation of proximal dendrites of the mutant by multiple CFs and ectopic PFs. *A–C*, Three spines (*1~*3) on the same shaft dendrite (PCD) are shown to contact with BDA-labeled/VGluT2-labeled CF (aCF), BDA-unlabeled/VGluT2-labeled CF (uCF), and PF (PF). In these transverse sections, PFs are identified as longitudinal axons parallel to the section plane and immunonegative terminals for BDA and VGluT2. A symmetric axodendritic synapse is also present and is judged as an interneuron terminal (Int). *D*, Reconstructed image for a proximal dendritic segment starting from the base of the primary dendrite upwards. PCD, Purkinje cell dendrite. Scale bar (in *A*), 500 nm.

We also examined the basic properties of PF-mediated EPSC (PF-EPSC). The 10–90% rise time and the decay time constant were similar between control and the α1A knock-out mouse at P18–P29 (Table 1). In the two stains of mice, PF-EPSC exhibited paired-pulse facilitation. The extent of facilitation was greater in the α1A knock-out mouse at interpulse intervals $<$50 msec (Fig. 7*B*). The coefficient of variation for the amplitude of PF-EPSC was slightly larger in the mutant mouse than in the control mouse (data not shown). These lines of evidence suggest that glutamate release from PF terminals is impaired in the VDCC α1A knock-out mouse, which is analogous to the phenotypes of the tottering and the rolling Nagoya (Matsushita et al., 2002). The severity of ataxia in these mice carrying α1A mutation appears to be correlated in part with the impairment of PF to PC transmission (Matsushita et al., 2002).

To check whether the changes in excitatory transmission resulted from the delay of maturation in the α1A knock-out mouse, we compared the data from the younger (P18–P22) and older (P28) mice. However, we did not see any significant difference between the two age groups with respect to 10–90% rise time, decay time constant, chord conductance, and paired-pulse ratio for either CF-EPSC or PF-EPSC (data not shown). It is therefore unlikely that the delay of maturation is a major cause of aforementioned abnormalities in the mutant mouse. Together, we conclude that the lack of VDCC α1A causes relatively minor changes in the basic properties of excitatory synaptic transmission in the cerebellum.

Discussion

The VDCC α1A subunit is expressed in various neurons (Westenbroek et al., 1995) and is known to regulate membrane excitability, gene expression, and neurotransmitter release (Miller, 1987; Llinas, 1988; Jun et al., 1999). In the present study, we studied the α1A knock-out mouse neuroanatomically and neurophysiologically to pursue its potential importance in cerebellar development. We disclosed another important function of the VDCC α1A subunit, namely, that it plays crucial roles in competitive synapse formation in PCs.

Abnormalities of PF synapses in the VDCC α1A knock-out mouse (i.e., enlargement and multiple contacts of PF terminals and their ectopic innervation to proximal dendrites) are consistent with previous reports on the spontaneous α1A mutant mice tottering, leaner, and rolling Nagoya (Rhyu et al., 1999a,b). We have also shown that ectopic PF synapses are formed on to PC somata. Thus, the PF territory is expanded proximally to cover all of the somatodendritic elements. Conversely, CFs of the VDCC α1A knock-out mouse are stunted in the molecular layer and do not innervate the distal portion of proximal dendrites, resulting in a diminished CF territory. Massive somatic innervation by CFs remains in mutant PCs at P21, a stage when it is almost eliminated in control PCs. On the basis of these observations, we conclude that the VDCC α1A subunit is a key molecule that fuels heterosynaptic competition, which works to the advantage of

Table 1. Basic properties of CF-EPSCs and PF-EPSCs

Genotype		10–90% Rise time (msec)	Decay time constant (msec)	Chord conductance (hp = −20 → +40 mV) (nS)	*n*
CF-EPSC					
Control	CF-mono	0.37 ± 0.04	6.1 ± 2.2	122.0 ± 65.7	18
	CF-multi-S	0.38 ± 0.05	5.9 ± 1.8	116.0 ± 78.8	11
	CF-multi-W	0.42 ± 0.11	3.6 ± 1.7	26.7 ± 25.1	10
α1A (−/−)	CF-mono	0.39 ± 0.07	7.1 ± 2.5	146.9 ± 56.1	7
	CF-multi-S	0.43 ± 0.06*	7.8 ± 2.1*	133.0 ± 60.8	24
	CF-multi-W	0.43 ± 0.11	3.0 ± 1.6	21.5 ± 19.0	46
PF-EPSC					
Control		1.09 ± 0.24	9.1 ± 3.0		15
α1A (−/−)		1.00 ± 0.25	9.0 ± 2.3		12

Data are expressed as mean ± SD. *$p < 0.05$ (*t* test), compared with the corresponding values of CF-multi-S from the control mice.

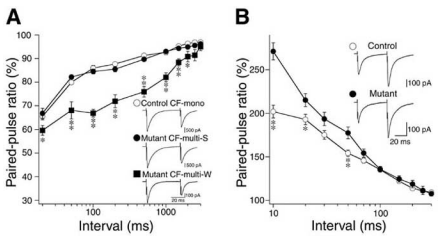

Figure 7. Paired-pulse plasticity of CF and PF synapses. *A*, Paired-pulse depression of CF-EPSCs for CF-mono in control PCs (open circles; 11 CFs) and for CF-multi-S (filled boxes; 12 CFs) and CF-multi-W (filled circles; 10 CFs) in mutant PCs. The amplitude of the second response is expressed as percentage of the first response (mean ± SEM) and is plotted as a function of interpulse intervals. Stimulus pairs were applied at 0.2 Hz. Insets are examples of CF-EPSCs for the three classes of CFs with an interpulse interval of 50 msec. Three traces are averaged. Holding potential was −20 mV. Records for CF-multi-S and CF-multi-W were obtained from the same mutant PCs. *B*, Paired-pulse facilitation of PF-EPSCs in control (open circles; 15 PCs) and mutant (filled boxes; 17 PCs) mice, which is illustrated similarly to *A*. Stimulus pairs were applied at 0.5 Hz. Insets are examples of PF-EPSCs with an interpulse interval of 50 msec. Ten consecutive traces are averaged at a holding potential of −80 mV. *$p < 0.05$; **$p < 0.01$.

CFs. This phenotypic alteration contrasts sharply with that reported for mice defective in GluRδ2, a molecule specific to the PF-PC synapse (Landsend et al., 1997). In GluRδ2-deficient PCs, numerous spines on spiny branchlets become free of PF innervation, and CF innervation is expanded distally to take over the free spines (Guastavino et al., 1990; Kashiwabuchi et al., 1995; Kurihara et al., 1997; Hashimoto et al., 2001; Lalouette et al., 2001; Ichikawa et al., 2002). This indicates that GluRδ2 fuels heterosynaptic competition to be advantageous to PFs. From these contrasting phenotypes, it is very likely that the properly structured synaptic wiring along the proximal-to-distal dendritic axis is achieved primarily through the balancing of the two distinct mechanisms. Because of their intense competition, the loss of one mechanism during synaptogenesis leads to the reduction of the territory supported by that mechanism and allows reciprocal expansion of the other.

Another notable phenotype of the VDCC α1A knock-out mouse is a high degree of persistent multiple CF innervation. Electrophysiological examination revealed that PCs innervated by multiple CFs comprise at least 83% of the total recorded PCs in the mutant mouse. Such a severe entanglement of the olivocerebellar projection may be the reason for the severe ataxia common to α1A-defective mice (Noebels and Sidman, 1979; Fletcher et al., 1996; Doyle et al., 1997; Jun et al., 1999) and humans (Ophoff et al., 1996). Anterograde tracer labeling confirms the severe multiple innervation and also reveals that it is caused by mixed innervation on the same soma and the same proximal dendrites of PCs. It is therefore likely that the other important role of the VDCC α1A subunit in PC synaptogenesis is to fuel homosynaptic competition among multiple CFs. Without this function, weaker CFs that would normally be eliminated can persist together with stronger CFs on the same somatodendritic compartments. In contrast, different patterns of multiple CF innervation have been demonstrated in other types of gene knock-out mice. In the majority of PCs from the GluRδ2 knock-out mouse, a single main CF establishes dominant innervation over proximal stem dendrites, whereas additional CFs arising from the neighbor innervate small portions of spiny branchlets (Hashimoto et al., 2001; Ichikawa et al., 2002). In a minor population of PCs from the GluRδ2 knock-out mouse, multiple CFs appear to innervate different dendritic branches (Hashimoto et al., 2002). In multiply innervated PCs from the adult mGluR1 knock-out mouse, a single main CF extensively innervates proximal dendrites, whereas one or two additional CFs weakly innervate restricted portions of proximal dendrites near the soma (K.H. and M.K., unpublished observation). These distinct forms of persistent multiple CF innervation indicate that the elimination of surplus CFs during cerebellar development requires coordinated actions of multiple molecular mechanisms. Our results suggest that VDCC α1A subunit may play key roles in consolidating the innervation by a single main CF and also in expelling surplus CFs from its innervation territory.

Despite the significant regression of the CF innervation territory and the severe impairment of developmental CF synapse elimination, the basic properties of CF-EPSCs appeared to be normal. In addition, despite the remarkable morphological changes in the PF terminals, the alteration of PF-PC synaptic transmission was relatively mild. These results were unexpected because the P/Q-type is the major Ca^{2+} channel subtype for neurotransmitter release from CF and PF terminals (Mintz et al., 1992, 1995; Matsushita et al., 2002). It was shown that N- and L-type VDCCs are augmented in PCs isolated from the VDCC α1A knock-out cerebellum (Jun et al., 1999). It was also reported that hippocampal synaptic transmission in the VDCC α1A knock-out mouse is altered such that transmitter release is mediated almost entirely by N-type VDCC (Jun et al., 1999). Therefore, it is likely that the lack of VDCC α1A at CF and PF terminals is compensated by an upregulation of other Ca^{2+} channel subtypes (Jun et al., 1999; Leenders et al., 2002; Matsushita et al., 2002). This could explain the very mild, at the most, functional alterations in CF and PF synapses. Thus, the changes in synaptic organizations of the VDCC α1A knock-out cerebellum seem un-

likely to result primarily from dysfunctional transmitter release from PFs or CFs.

We instead propose that the drastic alteration in the synaptic organization of the PCs is caused by impaired postsynaptic Ca^{2+} channel functions, although information is still lacking as to whether and how the loss of postsynaptic P/Q-type VDCC is compensated. The α1A subunit constitutes the high voltage-activated type of Ca^{2+} channels and is particularly abundant in PC somata and dendrites, constituting >90% of the total Ca^{2+} current density (Mintz et al., 1992, 1995; Stea et al., 1994). CF activity causes strong depolarization of PCs in an all-or-none manner and invariably elicits a characteristic complex spike (Eccles et al., 1966). Therefore, the Ca^{2+} influx into PCs during CF activity is primarily attained through VDCC formed by the α1A subunit. We assumed that CF-evoked Ca^{2+} influx to a PC through α1A channels may consolidate coactivated CF synapses, whereas it may punish other excitatory synapses unrelated to the Ca^{2+} influx. This proposed mechanism is reminiscent of the NMDA receptor-dependent synapse refinement in the visual and somatosensory systems, in which NMDA receptors are thought to function as a coincidence detector that introduces Ca^{2+} influx in an activity-dependent manner. It is thought that the Ca^{2+} influx through NMDA receptors strengthens synapses with correlated activities, whereas it weakens those with uncorrelated activities, through which immature redundant connections are refined into functionally mature ones (Lisman, 1989; Li et al., 1994; Feldman et al., 1998). Because cerebellar PCs lack NMDA receptors (Yamada et al., 2001), the VDCC α1A subunit may function as a substitute for the roles played by the NMDA receptors and may function as a coincidence detector. Without such Ca^{2+} channel function, activity-dependent shaping of functional synaptic circuitry is impaired; in the cerebellum, multiple CFs of different origins and PFs can be wired onto the same somatodendritic compartment. Therefore, we hypothesize that postsynaptic P/Q-type Ca^{2+} channels in PCs fuel heterosynaptic competition for extending the CF innervation territory along the PC dendritic tree and also fuel homosynaptic competition for establishing the monoinnervation by a main single CF of each PC. This should be tested in future studies using the PC-specific knock out of the α1A subunit gene.

References

Altman J (1972) Postnatal development of the cerebellar cortex in the rat. II. Phases in the maturation of Purkinje cells and of the molecular layer. J Comp Neurol 145:399–463.

Bravin M, Rossi F, Strata P (1995) Different climbing fibres innervate separate dendritic regions of the same Purkinje cell in hypogranular cerebellum. J Comp Neurol 357:395–407.

Bravin M, Morando L, Vercelli A, Rossi F, Strata P (1999) Control of spine formation by electrical activity in the adult rat cerebellum. Proc Natl Acad Sci USA 96:1704–1709.

Chedotal A, Sotelo C (1992) Early development of the olivocerebellar projections in the fetal rat using CGRP-immunocytochemistry. Eur J Neurosci 4:1159–1179.

Crepel F, Delhaye-Bouchaud N, Guastavino JM, Sampaio I (1980) Multiple innervation of cerebellar Purkinje cells by climbing fibers in *staggerer* mutant mouse. Nature 283:483–484.

Crepel F, Delhaye-Bouchaud N, Dupont JL (1981) Fate of the multiple innervation of cerebellar Purkinje cells by climbing fibers in immature control, X-irradiated and hypothyroid rats. Dev Brain Res 1:59–71.

Doyle J, Ren X, Lennon G, Stubbs L (1997) Mutations in the *Cacnl1a4* calcium channel gene are associated with seizures, cerebellar degeneration, and ataxia in tottering and leaner mutant mice. Mamm Genome 8:113–120.

Eccles JC, Llinas R, Sasaki K (1966) The excitatory synaptic action of climbing fibres on the Purkinje cells of the cerebellum. J Physiol (Lond) 182:268–296.

Feldman DE, Nicoll RA, Malenka RC, Isaac JTR (1998) Long-term depression at thalamocortical synapses in developing rat somatosensory cortex. Neuron 21:347–357.

Fletcher CF, Lutz CM, O'Sullivan TN, Shaughnessy Jr JD, Hawkes R, Frankel WN, Copeland NG, Jenkins NA (1996) Absence epilepsy in tottering mutant mice is associated with calcium channel defects. Cell 87:607–617.

Fremeau Jr RT, Troyer MD, Pahner I, Nygaad GO, Tran CH, Reimer RJ, Belloccio EE, Fortin D, Storm-Mathisen J, Edwards RH (2001) The expression of vesicular glutamate transporters defines two classes of excitatory synapse. Neuron 31:247–260.

Guastavino JM, Sotelo C, Damez-Kinselle I (1990) Hot-foot murine mutation: behavioral effects and neuroanatomical alterations. Brain Res 523:199–210.

Hashimoto K, Kano M (2003) Functional differentiation of multiple climbing fiber inputs during synapse elimination in the developing cerebellum. Neuron 38:785–796.

Hashimoto K, Ichikawa R, Takechi H, Inoue Y, Aiba A, Sakimura K, Mishina M, Hashikawa T, Konnerth A, Watanabe M, Kano M (2001) Roles of glutamate receptor δ2 subunit (GluRδ2) and metabotropic glutamate receptor subtype1 (mGluR1) in climbing fiber synapse elimination during postnatal cerebellar development. J Neurosci 21:9701–9712.

Ichikawa R, Miyazaki T, Kano M, Hashikawa T, Tatsumi H, Sakimura K, Mishina M, Inoue Y, Watanabe M (2002) Distal extension of climbing fiber territory and multiple innervation caused by abberant wiring to adjacent spiny branchlets in cerebellar Purkinje cells lacking glutamate receptor δ2. J Neurosci 22:8487–8503.

Ichise T, Kano M, Hashimoto K, Yanagihara D, Nakao K, Shigemoto R, Katsuki M, Aiba A (2000) mGluR1 in cerebellar Purkinje cells essential for long-term depression synapse elimination and motor coordination. Science 288:1832–1835.

Ito M (2001) Cerebellar long-term depression: characterization, signal transduction, and functional roles. Physiol Rev 81:1143–1195.

Jun K, Piedras-Renteria ES, Smith SM, Wheeler DB, Lee SB, Lee TG, Chin H, Adams ME, Scheller RH, Tsien RW, Shin HS (1999) Ablation of P/Q-type Ca^{2+} channel currents, altered synaptic transmission, and progressive ataxia in mice lacking the α_{1A}-subunit. Proc Natl Acad Sci USA 96:15245–15250.

Kakizawa S, Yamada K, Iino M, Watanabe M, Kano M (2003) Effects of insulin-like growth factor I on climbing fibre synapse elimination during cerebellar development. Eur J Neurosci 17:545–554.

Kano M, Rexhausen U, Dreessen J, Konnerth A (1992) Synaptic excitation produces a long-lasting rebound potentiation of inhibitory synaptic signals in cerebellar Purkinje cells. Nature 356:601–604.

Kano M, Hashimoto K, Chen C, Abeliovich A, Aiba A, Kurihara H, Watanabe M, Inoue Y, Tonegawa S (1995) Impaired synapse elimination during cerebellar development in PKCγ mutant mice. Cell 83:1223–1231.

Kano M, Hashimoto K, Kurihara H, Watanabe M, Inoue Y, Aiba A, Tonegawa S (1997) Persistent multiple climbing fiber innervation of cerebellar Purkinje cells in mice lacking mGluR1. Neuron 18:71–79.

Kano M, Hashimoto K, Watanabe M, Kurihara H, Offermanns S, Jiang H, Wu Y, Jun K, Shin HS, Inoue Y, Simon MI, Wu D (1998) Phospholipase Cβ4 is specifically involved in climbing fiber synapse elimination in the developing cerebellum. Proc Natl Acad Sci USA 95:15724–15729.

Kashiwabuchi N, Ikeda K, Araki K, Hirano T, Shibuki K, Takayama C, Inoue Y, Kutsuwada T, Yagi T, Kang Y, Aizawa S, Mishina M (1995) Impairment of motor coordination Purkinje cell synapse formation and cerebellar long-term depression in GluRδ2 mutant mice. Cell 81:245–252.

Konnerth A, Dreessen J, Augustine GJ (1992) Brief dendritic calcium signals initiate long-lasting synaptic depression in cerebellar Purkinje cells. Proc Natl Acad Sci USA 89:7051–7055.

Kurihara H, Hashimoto K, Kano M, Takayama C, Sakimura K, Mishina M, Inoue Y, Watanabe M (1997) Impaired parallel fiber-Purkinje cell synapse stabilization during cerebellar development of mutant mice lacking the glutamate receptor δ2 subunit. J Neurosci 17:9613–9623.

Laloutette A, Lohof A, Sotelo C, Guenet J, Mariani J (2001) Neurobiological effects of a mull mutation depend on genetic context: comparison between two hotfoot alleles of the delta-2 ionotropic glutamate receptor. Neuroscience 105:443–455.

Landsend AS, Amiry-Moghaddam M, Matsubara A, Bergersen L, Usami S, Wenthold RJ, Ottersen OP (1997) Differential localization of δ gluta-

mate receptors in the rat cerebellum: coexpression with AMPA receptors in parallel fiber-spine synapses and absence from climbing fiber-spine synapses. J Neurosci 17:834–842.

Larramendi LMH, Victor T (1967) Synapses on the Purkinje cell spines in the mouse an electronmicroscopic study. Brain Res 5:15–30.

Leenders AGM, van den Maagdenberg AMJM, Lopes da Silva FH, Sheng ZH, Molenaar PC, Ghijsen WEJM (2002) Neurotransmitter release from tottering mice nerve terminals with reduced expression of mutated P- and Q-type Ca^{2+}-channels. Eur J Neurosci 15:13–18.

Li Y, Erzurumlu RS, Chen C, Jhaveri S, Tonegawa S (1994) Whisker-related neuronal patterns fail to develop in the trigeminal brainstem nuclei of NMDAR1 knock-out mice. Cell 76:427–437.

Lisman J (1989) A mechanism for the Hebb and the anti-Hebb processes underlying learning and memory. Proc Natl Acad Sci USA 86:9574–9578.

Llinas RR (1988) The intrinsic electrophysiological properties of mammalian neurons: insights into central nervous system function. Science 242:1654–1664.

Mariani J (1982) Extent of multiple innervation of Purkinje cells by climbing fibers in the olivocerebellar system of weaver, reeler, and staggerer mutant mice. J Neurobiol 13:119–126.

Mariani J, Changeux JP (1981a) Ontogenesis of olivocerebellar relationships. I. Studies by intracellular recordings of the multiple innervation of Purkinje cells by climbing fibers in the developing rat cerebellum. J Neurosci 1:696–702.

Mariani J, Changeux JP (1981b) Ontogenesis of olivocerebellar relationships. II. Spontaneous activity of inferior olivary neurons and climbing fiber mediated activity of cerebellar Purkinje cells in developing rats. J Neurosci 1:703–709.

Matsushita K, Wakamori M, Rhyu IJ, Arii T, Oda S, Mori Y, Imoto K (2002) Bidirectional alterations in cerebellar synaptic transmission of *tottering* and *rolling* Ca^{2+} channel mutant mice. J Neurosci 22:4388–4398.

Miller RJ (1987) Multiple calcium channels and neuronal function. Science 235:46–52.

Mintz IM, Venema VJ, Swiderek KM, Lee TD, Bean BP, Adams ME (1992) P-type calcium channels blocked by the spider toxin ω-Aga-IVA. Nature 355:827–829.

Mintz IM, Sabatini BL, Regehr WG (1995) Calcium control of transmitter release at a cerebellar synapse. Neuron 15:675–688.

Miyazaki T, Fukaya M, Shimizu H, Watanabe M (2003) Subtype switching of vesicular glutamate transporters at parallel fibre-Purkinje cell synapses in developing mouse cerebellum. Eur J Neurosci 17:2563–2572.

Nakagawa S, Watanabe M, Isobe T, Kondo H, Inoue Y (1998) Cytological compartmentalization in the staggerer cerebellum, as revealed by calbindin immunohistochemistry for Purkinje cells. J Comp Neurol 395:112–120.

Noebels JL, Sidman RL (1979) Inherited epilepsy: spike-wave and focal motor seizures in the mutant mouse tottering. Science 204:1334–1336.

Offermanns S, Hashimoto K, Watanabe M, Sun W, Kurihara H, Thompson RF, Inoue Y, Kano M, Simon MI (1997) Impaired motor coordination and persistent multiple climbing fiber innervation of cerebellar Purkinje cells in mice lacking Gαq. Proc Natl Acad Sci USA 94:14089–14094.

Ophoff RA, Terwindt GM, Vergouwe MN, Van Eijk R, Oefner PJ, Hoffman SMG, Lamerdin JE, Mohrenweiser HW, Bulman DE, Ferrari M, Haan J, Lindhout D, van Ommen GJB, Hofker MH, Ferrari MD, Frants RR (1996) Familial hemiplegic migraine and episodic ataxia type-2 are caused by mutations in the Ca^{2+} channel gene CACNL1A4. Cell 87:543–552.

Palay S, Chan-Palay V (1974) Cerebellar cortex. Cytology and organization, pp 63–69, 242–287. New York: Springer.

Regehr WG, Mintz IM (1994) Participation of multiple calcium channel types in transmission at single climbing fiber to Purkinje cell synapses. Neuron 12:605–613.

Rhyu IJ, Abbott LC, Walker DB, Sotelo C (1999a) An ultrastructual study of granule cell/Purkinje cell synapses in tottering (*tg*/*tg*), leaner (tg^{la}/tg^{la}), and compound heterozygous tottering/leaner (*tg*/tg^{la}) mice. Neuroscience 90:717–728.

Rhyu IJ, Oda S, Uhm CS, Kim H, Suh YS, Abbott LC (1999b) Morphologic investigation of rolling mouse Nagoya (tg^{rol}/tg^{rol}) cerebellar Purkinje cells: anataxic mutant, revised. Neurosci Lett 266:49–52.

Sotelo C (1978) Purkinje cell ontogeny: formation and maintenance of spines. Prog Brain Res 48:149–170.

Stea A, Tomlinson WJ, Soong TW, Bourinet E, Dubel SJ, Vincent SR, Snutch TP (1994) Localization and functional properties of a rat brain α_{1A} calcium channel reflect similarities to neuronal Q- and P-type channels. Proc Natl Acad Sci USA 91:10576–10580.

Sugihara I, Bailly Y, Mariani J (2000) Olivocerebellar climbing fibers in the granuloprival cerebellum: morphological study of individual axonal projections in the X-irradiated rat. J Neurosci 20:3745–3760.

Westenbroek RE, Sakurai T, Elliott EM, Hell JW, Starr TVB, Snutch TP, Catterall WA (1995) Immunochemical identification and subcellular distribution of the α_{1A} subunits of brain calcium channels. J Neurosci 15:6403–6418.

Woodward DJ, Hoffer BJ, Altman J (1974) Physiological and pharmacological properties of Purkinje cells in rat cerebellum degranulated by postnatal x-irradiation. J Neurobiol 5:283–304.

Yamada K, Fukaya M, Shimizu H, Sakimura K, Watanabe M (2001) NMDA receptor GluRϵ1, GluRϵ3 and GluRζ1 are enriched at the mossy fibre-granule cell synapses in the adult mouse cerebellum. Eur J Neurosci 13:2025–2036.